


Efficient time-dependent orbital-free density functional theory: Semilocal adiabatic response

Kaili Jiang (姜凯立)^{1,*}, Xuecheng Shao (邵学成)^{1,†} and Michele Pavanello^{1,2,‡}

¹*Department of Chemistry, 73 Warren Street, Rutgers University, Newark, New Jersey 07102, USA*

²*Department of Physics, 101 Warren Street, Rutgers University, Newark, New Jersey 07102, USA*

 (Received 24 February 2022; revised 1 September 2022; accepted 2 September 2022; published 30 September 2022)

Orbital-free density functional theory and its time-dependent extension are efficient *ab initio* methods for calculating the electronic structure and dynamics of large systems. Through the calculation of the optical spectra of selected clusters, we reach three important conclusions: (1) The quality of the spectra is strongly affected by the quality of the corresponding ground-state electron density; (2) the adiabatic part of the electronic response to external perturbations can be safely evaluated at the semilocal level; and (3) the nonadiabatic, current-dependent part of the time-dependent Pauli potential is key to recover correct spectral envelopes.

DOI: [10.1103/PhysRevB.106.115153](https://doi.org/10.1103/PhysRevB.106.115153)

I. INTRODUCTION

In the quest for the development of accurate electronic structure methods capable of approaching those realistic microstates occurring in experiments, orbital-free density functional theory (OFDFT) is emerging as a tool for materials science and engineering [1,2]. The main distinction between OFDFT and the commonly adopted Kohn-Sham DFT (KSDFT) is the fact that in OFDFT, the orbital-dependent noninteracting kinetic energy is evaluated with an approximate, pure density functional. Even though the noninteracting kinetic energy is strictly a functional of the electron density (the Kohn-Sham orbitals are density functionals) its functional dependence on the electron density is yet unknown. Therefore, in OFDFT one needs two approximate functionals, one for the noninteracting kinetic energy (the so-called kinetic energy density functional, or KEDF) and one for the exchange-correlation (xc) functional. The accuracy of OFDFT is largely dominated by the accuracy of the KEDF employed.

KEDF approximants have historical roots in the Thomas-Fermi theory [3,4]. The simplest KEDF is a pure, local functional of the electron density function, namely,

$$T_S^{\text{TF}}[n] = C^{\text{TF}} \int d\mathbf{r} n^{5/3}(\mathbf{r}), \quad (1)$$

where C^{TF} is a constant. KEDFs have evolved to semilocal, generalized gradient approximation (GGA) functionals [5–9],

$$T_S^{\text{GGA}}[n] = C^{\text{TF}} \int d\mathbf{r} n^{5/3}(\mathbf{r}) F_t[s(\mathbf{r})], \quad (2)$$

where the reduced gradient $s(\mathbf{r}) = \frac{|\nabla n(\mathbf{r})|}{2(3\pi^2)^{1/3} n^{4/3}(\mathbf{r})}$ is the argument of the enhancement factor F_t . Similarly to functionals for the xc, the enhancement factor for KEDFs is typically given by $F_t(s) = 1 + F_t^{\text{P}}(s)$ [6] where for $s \rightarrow 0$ the enhancement

factor $F_t \rightarrow 1$ recovering the Thomas-Fermi functional for uniform densities and for $s < +\infty$ the Pauli enhancement factor $F_t^{\text{P}}(s)$ is nonzero. Nonlocal KEDFs are yet another category of functionals which depend on the value of the density in a *finite* neighborhood of a point \mathbf{r} . Several nonlocal KEDFs have the general form

$$T_S^{\text{NL}}[n] = \int d\mathbf{r} d\mathbf{r}' n^\alpha(\mathbf{r}) \omega[n](\mathbf{r} - \mathbf{r}') n^\beta(\mathbf{r}'). \quad (3)$$

Typically the kernel function $\omega[n](\mathbf{r} - \mathbf{r}')$ is approximated by a function of the electron density at point \mathbf{r} , and the magnitude of the distance between \mathbf{r} and \mathbf{r}' leading to simplified integrals involving convolutions which can be resolved in Fourier space with the aid of splines [10–12].

Employing many of the available KEDFs, OFDFT reproduces accurately the ground-state electronic structure of metallic systems [13] in part because the electronic structure of these systems resembles closely the one of the uniform electron gas which is the reference system for developing most KEDFs. Particularly for nonlocal KEDFs, the linear response of the free-electron gas is a constituting ingredient of the kernel [14]. For semiconductors, certain GGA [7,15] and nonlocal functionals [10,11] are able to describe semiquantitatively the ground state of only selected compounds (e.g., Si, and III-V compounds) whether in bulk, finite, or semi-infinite configurations.

Resting on early work [16–20], recent advances have showed that time-dependent OFDFT (TD-OFDFT) can be an accurate method for predicting the excited state dynamics and optical spectra of clusters [21–26]. The effective time-dependent potential in TD-OFDFT differs from the one of TD-DFT by the Pauli potential $v_{\text{P}}(\mathbf{r}, t)$, defined as the difference between the full KEDF potential and the von Weizsäcker (bosonic) potential,

$$v_{\text{P}}(\mathbf{r}, t) = v_{T_S}(\mathbf{r}, t) - v_{\text{vW}}(\mathbf{r}, t). \quad (4)$$

Because of the simplified (Madelung) wave function used in TD-OFDFT, there are strong nonadiabatic effects (i.e., frequency or history dependent) for the Pauli potential. In an

*kaili.jiang@rutgers.edu

†xuecheng.shao@rutgers.edu

‡m.pavanello@rutgers.edu

effort to account for such a nonadiabaticity, we and others have focused efforts on developing nonadiabatic Pauli potentials for TD-OFDFT simulations [25–28].

In this paper, we conveniently characterize the time dependence of the Pauli potential with two contributions: *Adiabatic*, recovered by evaluating functionals developed for the ground state with the time-dependent electron density as an argument; and *nonadiabatic*, defined as the discrepancy between the time dependence of the exact adiabatic Pauli potential and the exact potential.

Here, we analyze TD-OFDFT's optical spectra comparing them against conventional TD-DFT calculations. We do so invoking two aspects: the ability of OFDFT to reproduce the ground-state electron density $n_0(\mathbf{r})$ as well as the electron density response $\delta n(\mathbf{r}, t) = n(\mathbf{r}, t) - n_0(\mathbf{r})$. Following our analysis of the Pauli potential, we can also subdivide the density response into adiabatic and nonadiabatic. Thus, inspired by recent work from the Varga group [24], our analysis will center upon the detrimental effects on the predicted optical spectra of an approximate ground-state density recovered from the approximate KEDFs in comparison to the exact KSDFD density (for a given choice of xc functional), and the effect of several types of adiabatic Pauli potentials and whether or not a nonadiabatic correction derived from the uniform electron gas improves upon the adiabatic spectra. Our previous work shows that the nonadiabatic Pauli potential does improve the overall spectral envelope. However, in this paper we will be able to disentangle the various sources of error and quantify the effects of the approximations considered. The analysis will uncover an important opportunity, i.e., the possibility to use the adiabatic response from semilocal functionals in place of the more computationally expensive response from nonlocal functionals without losing accuracy in the predictions.

We remark that we take TD-DFT as a benchmark because it employs the exact noninteracting kinetic energy of N fermionic electrons, formally recovering the exact Pauli potential's adiabatic and nonadiabatic contributions. For consistency, we will use the same xc functional for OFDFT and KSDFD simulations throughout.

II. FORMALISM

In this section, we provide a brief introduction to the formalism behind TD-OFDFT. For more details, we refer the readers to Refs. [25,28,29]. In TD-OFDFT, one-to-one invertible maps are established between the real system of interacting electrons, the fictitious system of noninteracting electrons (also known as the KS system), and a fictitious system of noninteracting bosons. The bosonic system yields the following density–wave function relationship

$$n(\mathbf{r}, t) = N|\phi_B(\mathbf{r}, t)|^2, \quad (5)$$

where $\phi_B(\mathbf{r}, t)$ is a normalized bosonic wave function which can be expressed exactly as a Madlung-type wave function without loss of generality, $\phi_B(\mathbf{r}, t) = \sqrt{\frac{n(\mathbf{r}, t)}{N}} e^{iS(\mathbf{r}, t)}$. N is the number of electrons in the system. Throughout, the subscript B stands for bosonic system.

A time-dependent Schrödinger-like equation is employed to propagate the system for $t > t_0$ (atomic units are used throughout this work),

$$\left[-\frac{\nabla^2}{2} + v_B(\mathbf{r}, t) \right] \phi_B(\mathbf{r}, t) = i \frac{\partial}{\partial t} \phi_B(\mathbf{r}, t). \quad (6)$$

The time-dependent effective potential is given by

$$v_B(\mathbf{r}, t) = v_P(\mathbf{r}, t) + v_S(\mathbf{r}, t), \quad (7)$$

where $v_P(\mathbf{r}, t)$ is the time-dependent Pauli potential defined in Eq. (4), and $v_S(\mathbf{r}, t)$ is the time-dependent KS potential. The total Pauli potential can be represented as the adiabatic portion plus a nonadiabatic correction

$$v_P(\mathbf{r}, t) = v_P^{\text{ad}}(\mathbf{r}, t) + v_P^{\text{nad}}(\mathbf{r}, t), \quad (8)$$

where the adiabatic portion can be represented as the functional derivative of the Pauli energy with respect to the density at time t ,

$$v_P^{\text{ad}}(\mathbf{r}, t) = \left. \frac{\delta T_P[n_0]}{\delta n_0(\mathbf{r})} \right|_{n_0(\mathbf{r}) \rightarrow n(\mathbf{r}, t)}. \quad (9)$$

The Pauli energy is the difference between the noninteracting kinetic energy and the von Weizsäcker energy, $T_P[n] = T_S[n] - T_{\text{vW}}[n]$. Therefore, any kinetic energy functional can be used to approximate the adiabatic portion of the Pauli potential.

We disentangle the three parts of a time-dependent DFT simulation: (1) ground-state density $n_0(\mathbf{r})$, (2) adiabatic response, and (3) nonadiabatic response. We explore the effect of using several functionals of different complexity for the three parts: exact and approximate KEDFs (GGA or nonlocal) for predicting n_0 , GGA KEDF for approximating the adiabatic response, and the Jiang-Pavanello (JP) functional for approximating the nonadiabatic response.

Analysis of part (1) leads us to evaluate how the error in the ground-state density for approximate functionals affects the quality of TD-OFDFT spectra. Such a density-driven error should be reduced when a more accurate ground-state density is employed. We choose the initial condition of Eq. (6) to be $\phi_B(\mathbf{r}, 0) = \frac{1}{\sqrt{N}} \sqrt{n_0^{\text{KS}}(\mathbf{r})} e^{i\mathbf{k}\cdot\mathbf{r}}$ or $\phi_B(\mathbf{r}, 0) = \frac{1}{\sqrt{N}} \sqrt{n_0^{\text{LMGP}}(\mathbf{r})} e^{i\mathbf{k}\cdot\mathbf{r}}$, where $n_0^{\text{KS}}(\mathbf{r})$ and $n_0^{\text{LMGP}}(\mathbf{r})$ are the ground-state densities of the system of interest in KS-DFT and in OFDFT with the Local-kF Mi-Genova-Pavanello (LMGP) nonlocal functional [10], respectively, and $e^{i\mathbf{k}\cdot\mathbf{r}}$ denotes the momentum of strength $k = |\mathbf{k}|$ along the direction of the wave vector \mathbf{k} to the electronic system as the initial, weak perturbation. In this work, LMGP refers to LMGP0. For details regarding the different types of functionals in the LMGP family, we refer the readers to Ref. [10].

To analyze part (2), in a subsequent step, we solve the time-dependent Schrödinger-like equation in Eq. (6) with the adiabatic portion of the Pauli potential approximated with the following equation,

$$v_P^{\text{ad}}(\mathbf{r}, t) = v_P^{\text{GGA}}(\mathbf{r}, t) - v_P^{\text{GGA}}(\mathbf{r}, 0) + v_P^{\text{X}}(\mathbf{r}, 0), \quad (10)$$

where X is the Pauli potential from the KEDF used for the corresponding ground-state calculation (i.e., it can be either the exact KSDFD Pauli potential, or an approximate nonlocal

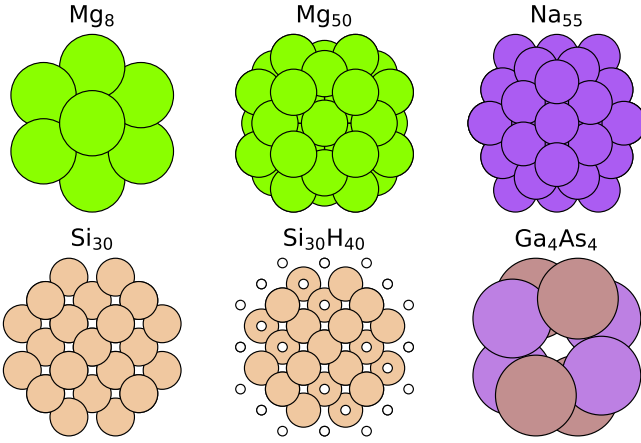


FIG. 1. The structures of the three systems used in calculations. Small white circles denote passivating hydrogen atoms [30,31] (see Supplemental Material for the structure files [30]).

or GGA Pauli potential). $v_p^{\text{GGA}}(\mathbf{r}, t)$ is the adiabatic Pauli potential evaluated using Eq. (9) at time t with T_p calculated from a GGA level functional approximation, and $v_p^{\text{GGA}}(\mathbf{r}, 0)$ is the Pauli potential evaluated with the same GGA functional using the ground-state density of X as its argument. In the KS case, a simple inversion is used to calculate the Pauli potential,

$$v_p^{\text{KS}}[n](\mathbf{r}) = \frac{\nabla^2 \sqrt{n(\mathbf{r})}}{2\sqrt{n(\mathbf{r})}} - v_s[n](\mathbf{r}), \quad (11)$$

which we find to be numerically stable for the systems considered.

Finally, part (3) of the analysis is carried out using the JP nonadiabatic correction of the Pauli potential developed recently by us [26], namely,

$$v_p^{\text{nad}}(\mathbf{r}, t) = -\frac{\pi^3}{12} \left(\frac{6}{k_F^2(\mathbf{r})} \mathcal{F}^{-1} \left\{ i\mathbf{q} \cdot \mathbf{j}(\mathbf{q}, t) \frac{1}{q} \right\} + \frac{1}{k_F^4(\mathbf{r})} \mathcal{F}^{-1} \{ i\mathbf{q} \cdot \mathbf{j}(\mathbf{q}, t) q \} \right), \quad (12)$$

where \mathbf{j} and \mathbf{q} are the electronic current density and the reciprocal space vector, respectively. The current density is determined by the standard equation $\mathbf{j}(\mathbf{r}) = \frac{1}{2i} [\phi^*(\mathbf{r}) \nabla \phi(\mathbf{r}) - \phi(\mathbf{r}) \nabla \phi^*(\mathbf{r})]$. \mathcal{F} stands for the Fourier transform and $k_F(\mathbf{r})$ is the Fermi wave-vector function of the local electron density.

III. COMPUTATIONAL DETAILS

We choose the following systems for our calculations: three metal clusters Mg_8 , Mg_{50} , and Na_{55} , and three semiconductor clusters Si_{30} , $\text{Si}_{30}\text{H}_{40}$, and Ga_4As_4 . The structures of the systems are illustrated in Fig. 1.

The TD-OFDFT calculations are performed with DFTpy [32] and the benchmark TD-DFT calculations are performed with embedded Quantum ESPRESSO's TD-DFT implementation [33–35]. All TD-OFDFT and TD-DFT calculations employ the same adiabatic Perdew-Zunger local density approximation (LDA) [36] as the xc functional and optimized effective pseudopotentials (OEPP) [37]. The kinetic energy cutoff for the TD-DFT wave functions and the TD-OFDFT

TABLE I. KSDFT-OFDFT density difference Δn_0 and energy difference ΔE_0 for the ground electronic state of the systems in Fig. 1, and energy difference in meV/electron. N stands for the total number of valence electrons in the systems.

System	N	LKT		LMGP	
		Δn_0	ΔE_0	Δn_0	ΔE_0
Mg_8	16	0.87	678	0.44	238
Mg_{50}	100	3.4	403	1.5	119
Na_{55}	55	4.0	73	2.9	235
Si_{30}	120	8.1	946	3.6	390
$\text{Si}_{30}\text{H}_{40}$	160	16.5	1158	4.8	180
Ga_4As_4	32	2.3	1324	1.0	412

density are chosen to converge the ground-state energy within 1 meV/atom, which is 104 eV for the Mg clusters, 150 eV for Na_{55} , 940 eV for the Si clusters, and 600 eV for Ga_4As_4 . The oscillator strength is calculated using $\sigma(\omega) = -\omega \text{Im}[\frac{\delta \tilde{\mu}(\omega)}{k}]$, where $\delta \tilde{\mu}(\omega)$ is the Fourier transform of the dipole moment change calculated at every time step of the propagation and k is the momentum, “kick” strength for the initial wave function, $\phi_B(\mathbf{r}, t=0)$ as described in the previous section. $k = 1.0 \times 10^{-3}$ a.u. is used for all calculations. The time step chosen is consistent with the plane-wave cutoff employed and is $dt = 0.1$ a.u. for the Mg, Na, and GaAs systems and $dt = 0.01$ a.u. for the Si systems.

As mentioned, we employ the following KEDFs: (1) GGA functional of Luo-Karasiev-Trickey (LKT) [7], which has the following Pauli enhancement factor [$F_t^{\text{P}}(s) = F_t(s) - \frac{2}{3}s^2$],

$$F_t^{\text{P}}(s) = \frac{1}{\cosh(as)}, \quad (13)$$

where $a = 1.3$; and (2) nonlocal functional LMGP [10].

A. Analysis of KEDF performance for the ground state

In Table I we report the ground-state electron density difference Δn_0 and the energy difference ΔE_0 between the KSDFT benchmark ground-state density and the approximate densities computed by OFDFT for the systems in Fig. 1. Δn_0 is defined with the following equation which has been used often in the OFDFT literature [10],

$$\Delta n_0 = \frac{1}{2} \int |n_{\text{KSDFT}}(\mathbf{r}) - n_{\text{OFDFT}}(\mathbf{r})| d\mathbf{r}. \quad (14)$$

In all systems considered, the nonlocal functional LMGP yields more accurate densities than the GGA functional LKT. We choose LKT in this work because it was shown to be among the best GGA functionals available to date [7]. While the LKT density is very good for metallic systems, the error becomes large for the semiconductor cluster $\text{Si}_{30}\text{H}_{40}$. This hints to the fact that LKT will suffer a large density-driven error for the ground state. This error may even carry over to the time-dependent simulations and result in errors in the predicted response properties, such as optical spectra. On the other hand, LMGP's performance is better for metallic systems than semiconductors, but the errors involved are smaller.

TABLE II. Comparison of static dipole polarizability, $\alpha_{xx}(\omega = 0)$ (a.u.).

KEDF for n_0	LKT	LKT	LMGP	LMGP	Exact	Exact	Exact
v_p for $\delta n(t)$	LKT	LKT+JP	LKT	LKT+JP	LKT	LKT+JP	Exact
Mg ₈	555	547	434	446	414	409	486
Mg ₅₀	2256	2149	1501	1519	1826	1817	1500
Na ₅₅	4391	4343	3433	3364	3175	3135	3537
Si ₃₀	1747	1727	1296	1280	1373	1361	1501
Si ₃₀ H ₄₀	2735	2706	1951	1928	1980	1962	1971
Ga ₄ As ₄	289	285	211	204	194	192	210

We also note that the LMGP energy is also generally better than the LKT energy except for the Na₅₅ system.

B. Analysis of KEDF performance for electronic structures out of equilibrium

To inspect the performance of TD-OFDFT for reproducing quantities related to the response of the system to external perturbations, in Table II we report the static dipole polarizabilities α_{xx} for the systems considered. The table is organized so that the ground-state density-driven error reduces in going from left to right.

We remind the reader that we are computing the electronic response exclusively with the adiabatic LKT functional utilizing Eq. (10) (LKT) with and without the corrective potential in Eq. (12) due to the nonadiabaticity of the Pauli potential (LKT+JP).

From the table we notice that the trends are very similar to the ones in Table I in that the quality of the computed quantity (in this case the dipole polarizability) increases as the ground-state density used is closer to the one from KSDFT (which employs the exact Pauli potential). This gives us hope that a GGA functional, such as LKT, can perform well in predicting the $\omega \neq 0$ response of an electronic system to external pertur-

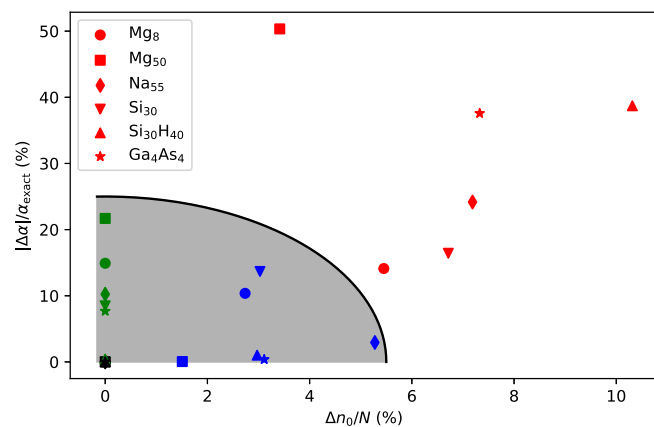


FIG. 2. Comparison of the errors in the dipole polarizability and the ground-state density. α is taken from Table II and δn_0 from Table I. All values except the black markers employ the LKT response. Black: TD-DFT response on top of the KSDFT density; green: LKT response on top of the KSDFT density; blue: LKT response on top of the LMGP density; red: LKT response on top of the LKT density. The black curve has been inserted to ease the interpretation of the scatter plot.

bations. Table II also shows that the nonadiabatic contribution to the Pauli potential only shifts the dipole polarizability by up to 70 a.u., or less than 2%.

To better analyze these results, we plot the values of Tables II and I in a scatter plot in Fig. 2. The figure clearly shows that dipole polarizabilities computed from the LKT ground-state density are worse than the ones computed with LMGP or KS ground-state densities.

Analyzing further Fig. 2 and Tables II and I we notice that in many cases polarizabilities computed from the LMGP ground-state density are closer to the benchmark KSDFT result than the ones computed from the exact (KS) density. This must be due to error cancellation. Let us explain the error cancellation with a simple truth table.

Considering the logic that emerges from Table III, when employing an approximate (OFDFT) ground-state density and then determining the response also approximately (OFDFT) results in a method that is more approximate than the method originating from starting from the KSDFT ground-state density and the approximate (OFDFT) response. Therefore, we can clearly and safely assign the apparently more accurate behavior of the dipole polarizabilities involving LMGP ground-state densities in comparison to those involving KSDFT ground-state densities to error cancellation. We also note that even though the ground-state energy values provided in Table I are interesting and useful to provide context to the approximations involved, they do not provide useful information to infer on the quality of excited state properties. Therefore, alongside the just presented dipole polarizabilities, we now move on to consider optical spectra in the next set of results.

To determine whether the same trend is recovered for time-dependent external perturbations, we also computed the optical spectra of the same clusters. In Figs. 3 and 4, we start

TABLE III. Truth table regarding the approximate or exact (within numerical precision) noninteracting kinetic energy given their dependence on a ground-state density n_0 and a density response $\delta n(t)$. As before, KSDFT is labeled as exact because it employs the exact noninteracting kinetic energy. OFDFT stands for approximate noninteracting kinetic energy employed in OFDFT simulations (in this work they are realized by the LKT and the LMGP kinetic energy functionals).

n_0	KSDFT	KSDFT	OFDFT
$\delta n(t)$	KSDFT	OFDFT	OFDFT
Noninteracting kinetic energy	Exact	Approx.	Approx.
No. of approximations	0	1	2

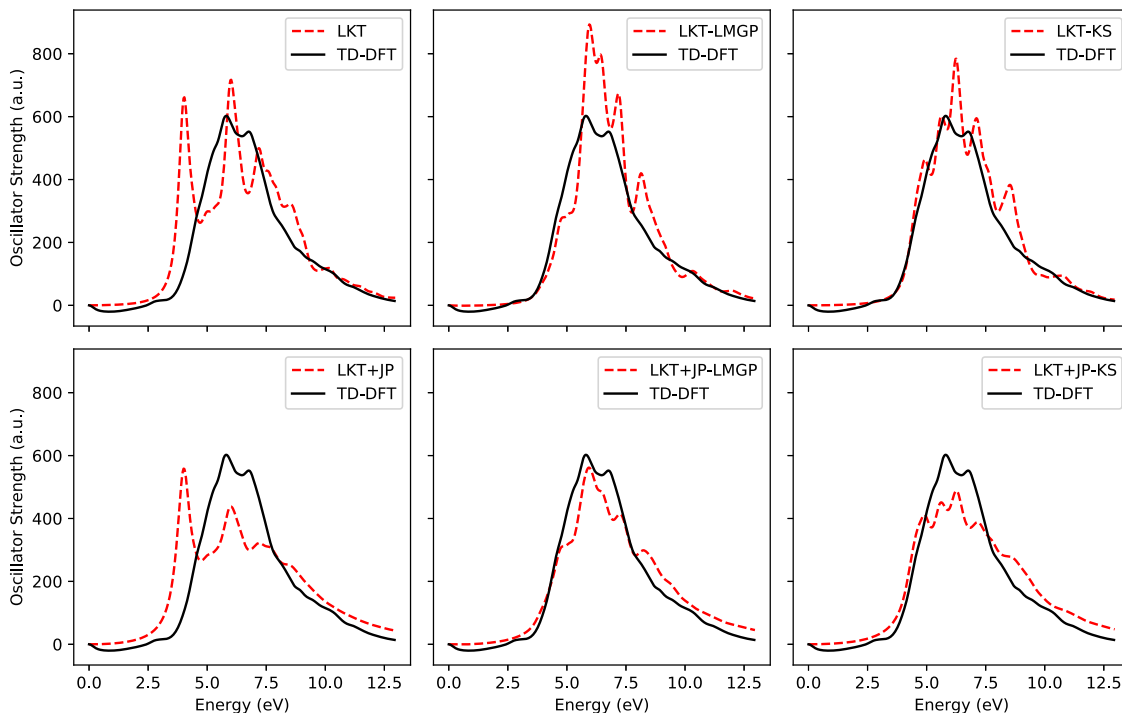


FIG. 3. Optical spectrum of the Mg_{50} cluster (see Fig. 1 for a snapshot of the structure). LKT is a GGA kinetic energy functional employed in the adiabatic approximation (i.e., $v_p(t) \simeq v_p[n_0 = n(t)]$). “+JP” stands for adiabatic LKT augmented by the additional propagation step with the nonadiabatic potential in Eq. (12). “-LMGP” and “-KS” stand for the LMGP or the KS ground-state density used as the initial condition instead of the LKT ground-state density, respectively.

by considering the optical spectrum of clusters of magnesium (Mg_{50} and Mg_8) analyzing the effect of using three different ground-state densities, LKT, LMGP, and KSDFT, only an adiabatic response (i.e., $\tilde{v}_p^{nad} = 0$), and including nonadiabaticity

in the Pauli potential at the level of the JP potential given in Eq. (12).

The adiabatic LKT response on the LKT ground-state density yields at best a qualitatively correct optical spectrum.

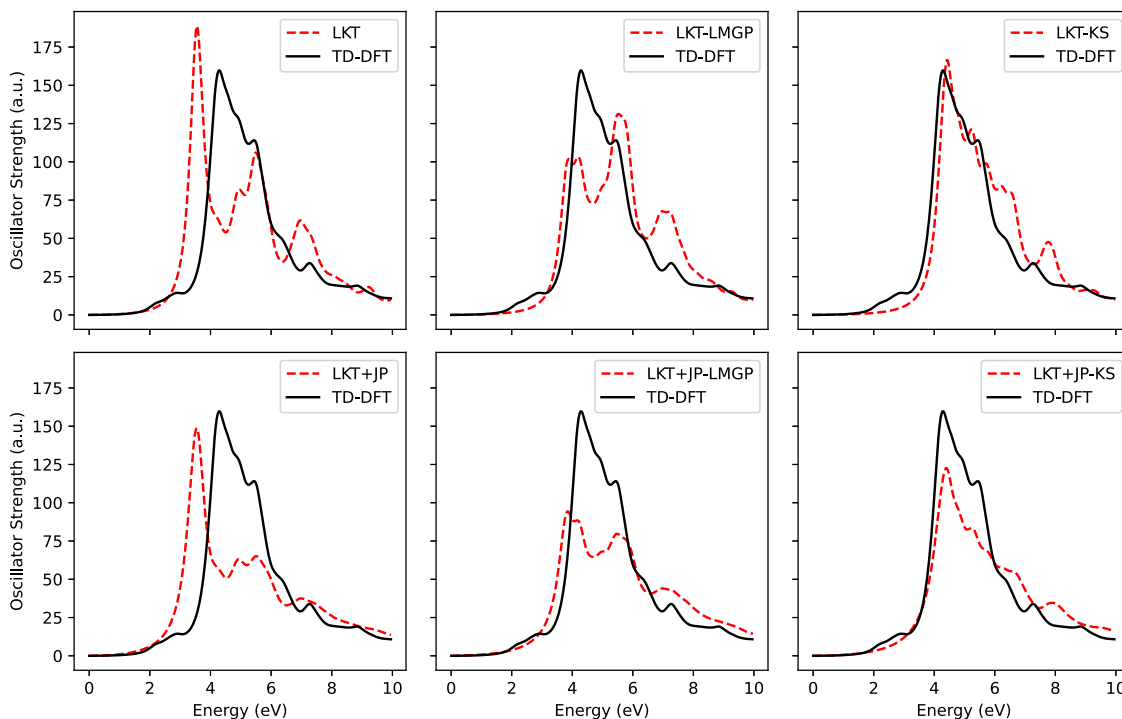


FIG. 4. Optical spectrum of the Mg_8 cluster. See caption to Fig. 3 for additional details.

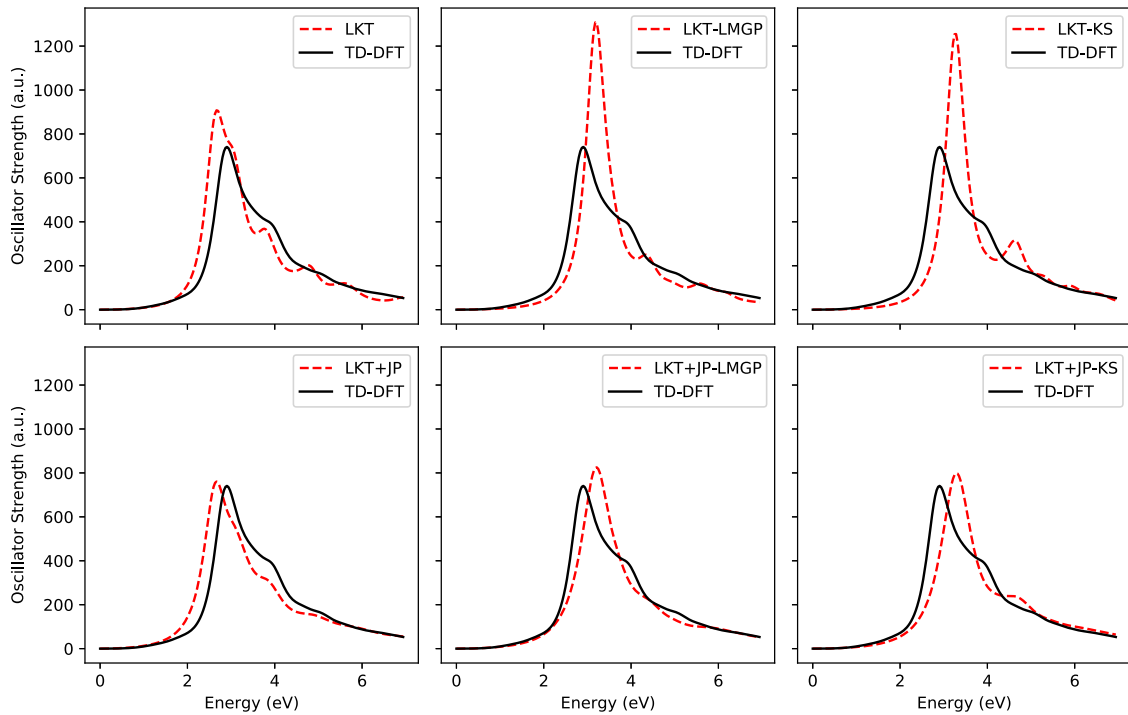


FIG. 5. Optical spectrum of the Na_{55} cluster. See caption to Fig. 3 for additional details.

Employing the more accurate LMGP or the KS ground-state density, the overall spectrum (peak positions, especially) is much closer to the TD-DFT benchmark, but the spectral envelope is not recovered fully. The addition of the nonadiabatic correction from the JP functional corrects the spectral envelope further. Thus, LMGP or KS ground-state density, LKT

adiabatic response, and a JP nonadiabatic correction delivers a TD-OFDFT result very close to the TD-DFT spectrum.

The magnesium clusters are a good example to show the interplay between the three error contributions (ground-state density, adiabatic, and nonadiabatic response). The majority of the error comes from a density-driven error, as indicated

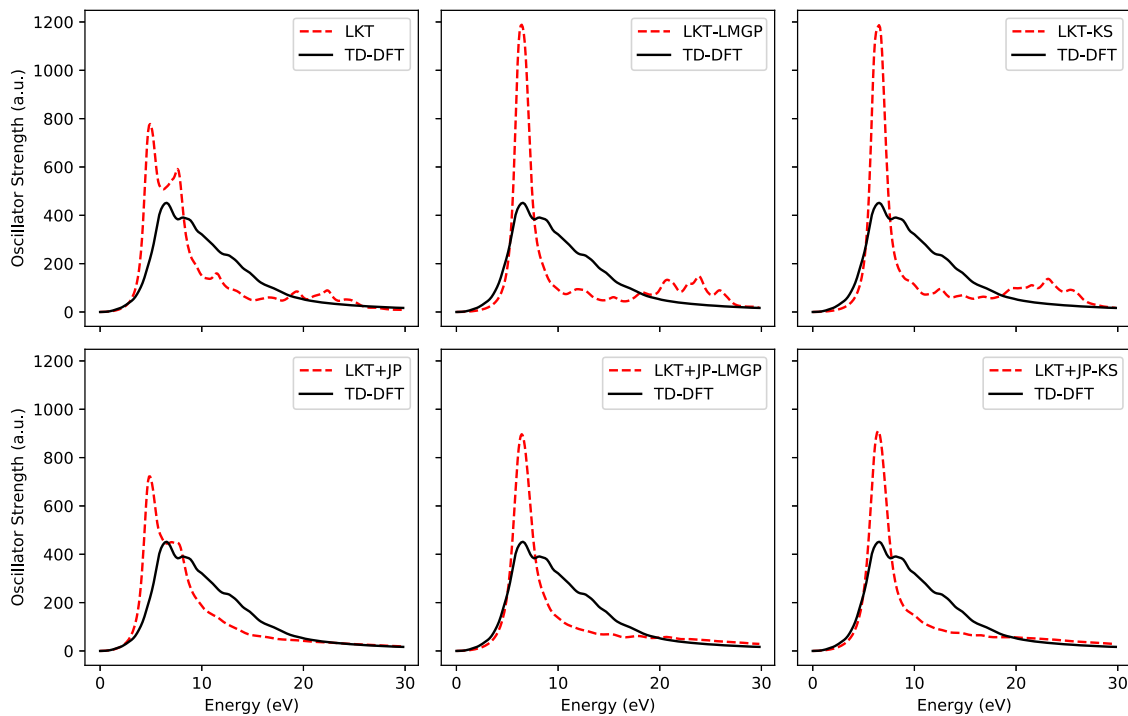


FIG. 6. Optical spectrum of the $\text{Si}_{30}\text{H}_{40}$ cluster. See caption to Fig. 3 for additional details.

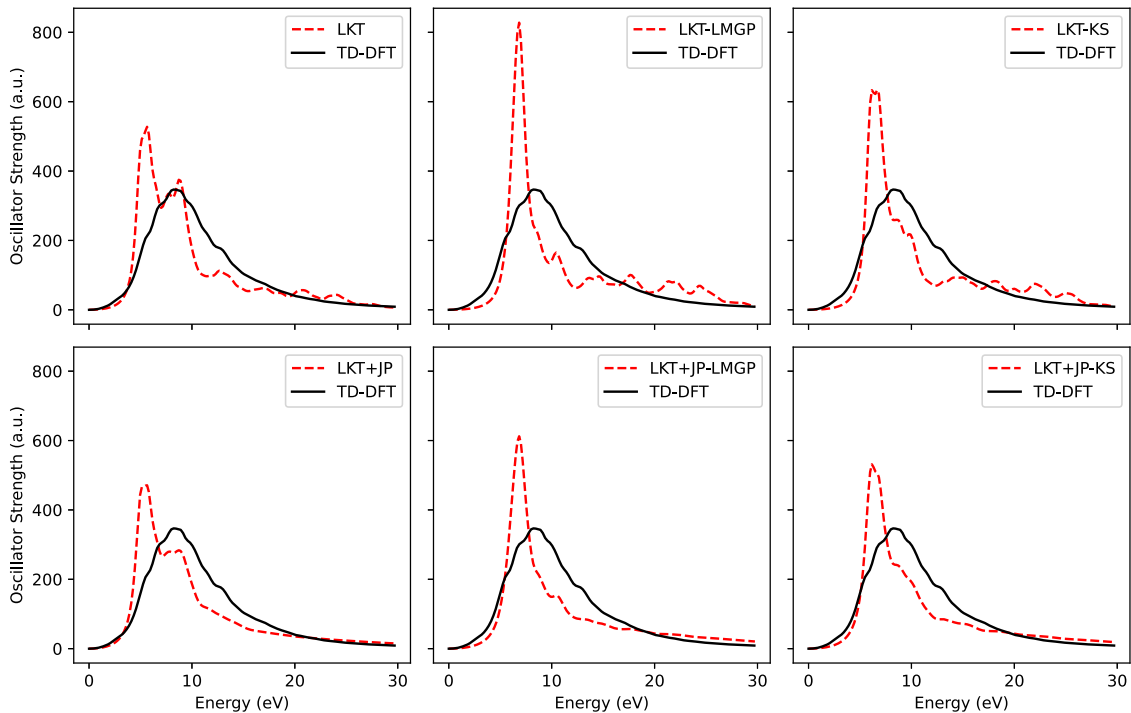


FIG. 7. Optical spectrum of the Si_{30} cluster. See caption to Fig. 3 for additional details.

by the massive improvement of the spectrum in going from using the LKT ground-state density to the LMGP and KS. The nonadiabatic functional-driven error mainly contributes to the shape of the spectral envelope.

Figures 5 and 6 report an analysis similar to the one done for the Mg_{55} cluster. It has been reported that TD-OFDFT yields accurate optical spectra for Na clusters even with the simple adiabatic Thomas–Fermi–von Weizsäcker approximation [21]. Here, we recover a similar behavior: The adiabatic LKT spectrum closely reproduces the TD-DFT result. However, this is due to massive error cancellations between the density-driven and functional-driven errors. The bottom right panel of Fig. 5 indicates that the nonadiabatic functional-driven error of LKT blueshifts the peak. The peak redshifts from the right panels to the left panels as the density-driven error is introduced. The strength of the peak also goes down. When we introduce nonadiabaticity in the Pauli potential, the spectral envelope is recovered fully (e.g., the largely overestimated peak strength for the peak at 3 eV is corrected).

A similar tale is recovered from analyzing the spectra of the silicon clusters ($\text{Si}_{30}\text{H}_{40}$ and Si_{30}) in Figs. 6 and 7. Unfortunately, in comparison to the two metal clusters, the errors are much larger. We note, especially, that the functional-driven error is very large because even including the nonadiabatic corrections to the Pauli potential delivers a spectrum that is not as close to the benchmark as the one of the metallic clusters considered previously.

In Fig. 8 we show that the response evaluated with LKT+JP and with LMGP+JP delivers similar spectra for the $\text{Si}_{30}\text{H}_{40}$ cluster. This shows that the problems for recovering the complete spectral envelope are rooted in the nonadiabatic part of the response. We expect such a behavior for semiconductors because the approximate KEDFs developed so far are parametrized/developed for metals. Additionally, the JP func-

tional is derived from the Lindhard function of the bosonic free-electron gas which also resembles more metallic systems than semiconductors. We witnessed a similar behavior for a large GaAs cluster in a recent related work [26] where we attributed the discrepancies between the TD-OFDFT and TD-DFT results to the absence in the JP potential of an account of interband transitions. However, despite the semiquantitative nature of the agreement with the benchmark TD-DFT result, Fig. 6 shows that by reducing the density-driven error, TD-OFDFT recovers the correct energy position of the main peak (plasmonic) in the spectrum.

In Fig. 9 we conduct the same analysis for a Ga_4As_4 cluster obtaining results in line with those for the Mg_{50} cluster. This further suggests that evaluating the LKT+JP response with

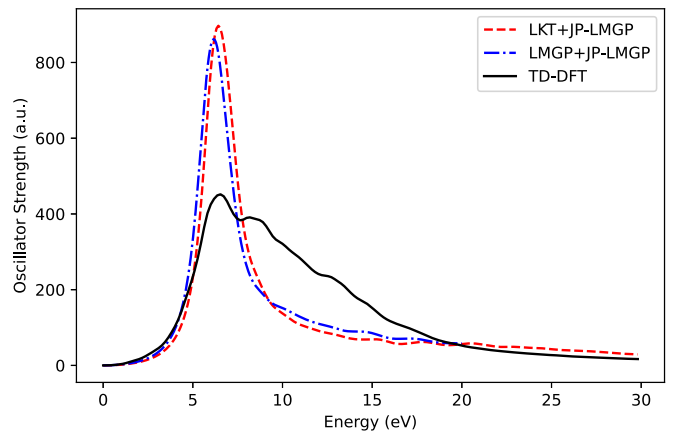


FIG. 8. Optical spectrum of the $\text{Si}_{30}\text{H}_{40}$ cluster comparing LMGP and LKT adiabatic response using in both cases the LMGP ground-state electron density and the JP nonadiabatic correction.

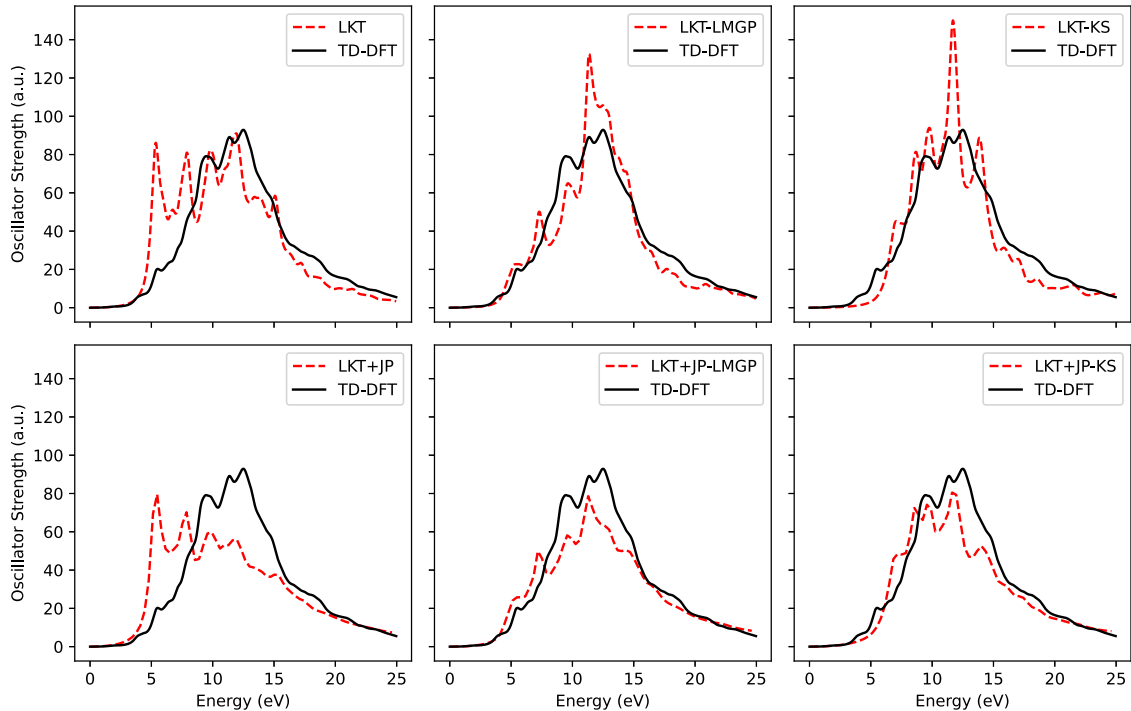


FIG. 9. Optical spectrum of the Ga_4As_4 cluster. See caption to Fig. 3 for additional details.

the KS ground-state density improves the predictivity of the TD-OFDFT simulations making them closer to the benchmark TDDFT optical spectra.

We carried out the same calculations with adiabatic response evaluated from the TFW functional (i.e., Thomas-Fermi functional used for the Pauli energy and potential) and found very similar results compared to the LKT response (see Supplemental Material for the TFW results [30]).

C. Computational cost

To understand why it is important to develop efficient TD-OFDFT methods based on the adiabatic response from GGA functionals, in Table IV we compare the computational wall time of TD-OFDFT simulations carried out with GGA (LKT) and nonlocal (LMGP) adiabatic responses for the Pauli potential with the computational time of the same TD-OFDFT methods on top of the KS “exact” density as well as the

TABLE IV. Wall times for OF-TDDFT and TD-DFT simulations on the six systems considered in this work measured in seconds \times CPU/step for a variety of methods. This table follows the nomenclature introduced in Table II.

KEDF for n_0 v_p for $\delta n(t)$	Exact LKT+JP	LMGP LMGP+JP	Exact Exact
Mg_8	3	16	32
Mg_{50}	4	49	674
Na_{55}	3	44	328
Si_{30}	17	163	197
$\text{Si}_{30}\text{H}_{40}$	23	210	446
Ga_4As_4	11	119	120

LMGP density. Overall, we see a two orders of magnitude reduction in computational cost with TD-DFT and a one order of magnitude reduction compared to using nonlocal KEDFs in TD-OFDFT as the system size used for this work. The TD-OFDFT computational cost is best for large systems as TD-OFDFT scales linearly with the system size. However, the computational cost for the KS ground-state density would also increase. Therefore, for very large systems it is better to use the ground-state density from nonlocal KEDFs as the initial condition.

IV. CONCLUSION

We propose time-dependent orbital-free DFT as a viable alternative to regular time-dependent DFT when large system sizes need to be modeled. In this paper, we explore the possibility of employing computationally cheap semilocal functionals for computing the adiabatic response to external perturbations and a current-dependent approximation for computing the nonadiabatic part of the response. Our simulations confirm that TD-OFDFT can quantitatively reproduce the spectra of metallic systems provided that the ground-state density is of good quality. The situation is more delicate when semiconductors are considered. In this case, the current-dependent nonadiabatic response derived from the uniform electron gas is not quantitative as it misses interband transitions. Our work sets the stage for using a GGA-level adiabatic response for the Pauli potential in OF-TDDFT simulations achieving one order of magnitude improvements for the computational time to solution compared to TD-OFDFT carried out with nonlocal Pauli potentials. Compared with standard TD-DFT, the timings are cut down by roughly two orders of magnitude.

ACKNOWLEDGMENTS

This work is supported by the U.S. Department of Energy, Office of Basic Energy Sciences, under Award No. DE-SC0018343. The authors acknowledge the Office of

Advanced Research Computing (OARC) at Rutgers, The State University of New Jersey for providing access to the Amarel and Caliburn clusters and associated research computing resources that have contributed to the results reported here [38].

-
- [1] W. C. Witt, B. G. del Rio, J. M. Dieterich, and E. A. Carter, Orbital-free density functional theory for materials research, *J. Mater. Res.* **33**, 777 (2018).
- [2] Y. A. Wang and E. A. Carter, Orbital-free kinetic-energy density functional theory, in *Theoretical Methods in Condensed Phase Chemistry* (Springer, Berlin, 2002), pp. 117–184.
- [3] L. H. Thomas, The calculation of atomic fields, *Math. Proc. Cambridge Philos. Soc.* **23**, 542 (1927).
- [4] E. Fermi, Un metodo statistico per la determinazione di alcune priorietà dell'atomo, *Atti Rend. Accad. Naz. Lincei* **6**, 602 (1927).
- [5] C. F. v. Weizsäcker, Zur Theorie der Kernmassen, *Z. Phys.* **96**, 431 (1935).
- [6] A. Lembarki and H. Chermette, Obtaining a gradient-corrected kinetic-energy functional from the Perdew-Wang exchange functional, *Phys. Rev. A* **50**, 5328 (1994).
- [7] K. Luo, V. V. Karasiev, and S. B. Trickey, A simple generalized gradient approximation for the noninteracting kinetic energy density functional, *Phys. Rev. B* **98**, 041111(R) (2018).
- [8] F. Tran and T. A. Wesolowski, Link between the kinetic- and exchange-energy functionals in the generalized gradient approximation, *Int. J. Quantum Chem.* **89**, 441 (2002).
- [9] S. Laricchia, E. Fabiano, L. A. Constantin, and F. Della Sala, Generalized gradient approximations of the noninteracting kinetic energy from the semiclassical atom theory: Rationalization of the accuracy of the frozen density embedding theory for nonbonded interactions, *J. Chem. Theory Comput.* **7**, 2439 (2011).
- [10] W. Mi and M. Pavanello, Orbital-free density functional theory correctly models quantum dots when asymptotics, nonlocality, and nonhomogeneity are accounted for, *Phys. Rev. B* **100**, 041105(R) (2019).
- [11] C. Huang and E. A. Carter, Nonlocal orbital-free kinetic energy density functional for semiconductors, *Phys. Rev. B* **81**, 045206 (2010).
- [12] L.-W. Wang and M. P. Teter, Kinetic-energy functional of the electron density, *Phys. Rev. B* **45**, 13196 (1992).
- [13] A. Aguado, D. J. González, L. E. González, J. M. López, S. Núñez, and M. J. Stott, An orbital free ab initio method: Applications to liquid metals and clusters, in *Recent Progress in Orbital-free Density Functional Theory* (World Scientific, Singapore, 2013), pp. 55–145.
- [14] Y. A. Wang, N. Govind, and E. A. Carter, Orbital-free kinetic-energy density functionals with a density-dependent kernel, *Phys. Rev. B* **60**, 16350 (1999).
- [15] L. A. Constantin, E. Fabiano, and F. Della Sala, Performance of semilocal kinetic energy functionals for orbital-free density functional theory, *J. Chem. Theory Comput.* **15**, 3044 (2019).
- [16] M. Horbatsch and R. M. Dreizler, Time dependent thomas fermi approach to atomic collisions I., *Z. Phys. A* **300**, 119 (1981).
- [17] P. Zimmerer, N. Grün, and W. Scheid, Trajectory method for time-dependent Thomas-Fermi equations and application to atoms in laser fields, *Phys. Lett. A* **134**, 57 (1988).
- [18] B. P. van Zyl and E. Zaremba, Thomas–Fermi–Dirac–von Weizsäcker hydrodynamics in laterally modulated electronic systems, *Phys. Rev. B* **59**, 2079 (1999).
- [19] M. Rusek, H. Lagarde, and T. Blenski, Cluster explosion in an intense laser pulse: Thomas-Fermi model, *Phys. Rev. A* **63**, 013203 (2000).
- [20] M. Pi, M. Barranco, J. Nemeth, C. Ngo, and E. Tomasi, Time-dependent Thomas-Fermi approach to nuclear monopole oscillations, *Phys. Lett. B* **166**, 1 (1986).
- [21] A. Doms, P.-G. Reinhard, and E. Suraud, Time-Dependent Thomas-Fermi Approach for Electron Dynamics in Metal Clusters, *Phys. Rev. Lett.* **80**, 5520 (1998).
- [22] H. Xiang, M. Zhang, X. Zhang, and G. Lu, Understanding quantum plasmonics from time-dependent orbital-free density functional theory, *J. Phys. Chem. C* **120**, 14330 (2016).
- [23] H. M. Baghramyan, F. Della Sala, and C. Ciraci, Laplacian-Level Quantum Hydrodynamic Theory for Plasmonics, *Phys. Rev. X* **11**, 011049 (2021).
- [24] C. Covington, J. Malave, and K. Varga, Coupled Maxwell and time-dependent orbital-free density functional calculations, *Phys. Rev. B* **103**, 075119 (2021).
- [25] K. Jiang and M. Pavanello, Time-dependent orbital-free density functional theory: Background and Pauli kernel approximations, *Phys. Rev. B* **103**, 245102 (2021).
- [26] K. Jiang, X. Shao, and M. Pavanello, Nonlocal and nonadiabatic Pauli potential for time-dependent orbital-free density functional theory, *Phys. Rev. B* **104**, 235110 (2021).
- [27] D. Neuhauser, S. Pistinner, A. Coomar, X. Zhang, and G. Lu, Dynamic kinetic energy potential for orbital-free density functional theory, *J. Chem. Phys.* **134**, 144101 (2011).
- [28] A. J. White, O. Certik, Y. H. Ding, S. X. Hu, and L. A. Collins, Time-dependent orbital-free density functional theory for electronic stopping power: Comparison to the Mermin-Kohn-Sham theory at high temperatures, *Phys. Rev. B* **98**, 144302 (2018).
- [29] W. L. Schaich, A hydrodynamic model calculation of linear and nonlinear optical response in an asymmetric parabolic quantum well, *Solid State Commun.* **88**, 5 (1993).
- [30] See Supplemental Material at <http://link.aps.org/supplemental/10.1103/PhysRevB.106.115153> for a collection of the structure files and the equivalents to Table 2 and Figs. 3–7 and 9 recalculated with adiabatic response from the TFW functional.
- [31] X. Huang, E. Lindgren, and J. R. Chelikowsky, Surface passivation method for semiconductor nanostructures, *Phys. Rev. B* **71**, 165328 (2005).
- [32] X. Shao, K. Jiang, W. Mi, A. Genova, and M. Pavanello, DFTpy: An efficient and object-oriented platform for orbital-

- free DFT simulations, *WIREs Comput. Mol. Sci.* **11**, e1482 (2021).
- [33] A. Genova, Jr., D. Ceresoli, A. Krishtal, O. Andreussi, R. A. DiStasio, and M. Pavanello, eQE: An open-source density functional embedding theory code for the condensed phase, *Int. J. Quantum Chem.* **117**, e25401 (2017).
- [34] W. Mi, X. Shao, A. Genova, D. Ceresoli, and M. Pavanello, eQE 2.0: Subsystem DFT beyond GGA functionals, *Comput. Phys. Commun.* **269**, 108122 (2021).
- [35] A. Krishtal, D. Ceresoli, and M. Pavanello, Subsystem real-time time dependent density functional theory, *J. Chem. Phys.* **142**, 154116 (2015).
- [36] J. P. Perdew and A. Zunger, Self-interaction correction to density-functional approximations for many-electron systems, *Phys. Rev. B* **23**, 5048 (1981).
- [37] W. Mi, S. Zhang, Y. Wang, Y. Ma, and M. Miao, First-principle optimal local pseudopotentials construction via optimized effective potential method, *J. Chem. Phys.* **144**, 134108 (2016).
- [38] <http://oarc.rutgers.edu>.